Supplementary Information for

DNA detection using a light-emitting polymer single nanowire

Dong Hyuk Park[ab], Nari Kim[b], Chunzhi Cui[b], Young Ki Hong[a], Mi Suk Kim[a], Doo-Ho Yang[b], Dae-Chul Kim[c], Hyunsoo Lee[c], Jeongyong Kim*[c], Dong June Ahn*[b] and Jinsoo Joo*[a]

[a]Department of Physics, Korea University, Seoul 136-713, Korea.

[b]Department of Chemical and Biological Engineering, Korea University, Seoul 136-713 Korea.

[c]Department of Physics, University of Incheon, Incheon 406-772, Korea.

*These authors contributed equally to this work. To whom correspondence should be addressed, E-mail: jjoo@korea.ac.kr. Tel: +82-2-3290-3103.

In this Supplementary Information, we present the following results:

(1) Detailed experimental procedures.

(2) Scanning electron microscopy (SEM) images of the P3MT, P3MT/*p*-DNA, and P3MT/ *p*-DNA+*t*-DNA NWs.

(3) Fourier transform infrared (FT-IR) absorption spectra of P3MT(DBSA), P3MT(DBSA)/ *p*-DNA, and P3MT(DBSA)/*p*-DNA+*t*-DNA NWs.

(4) Laser confocal microscopy (LCM) PL images of a single strand of P3MT(DBSA), P3MT(DBSA)/*p*-DNA, and P3MT(DBSA)/*p*-DNA+*t*-DNA NWs.

(5) Quantum yield (Φ_{QY}) of P3MT(DBSA), P3MT(DBSA)/*p*-DNA, and P3MT(DBSA)/*p*-DNA+*t*-DNA NWs.

(6) Comparative study using a single strand of dedoped-P3MT NWs.

(7) Study of solvent treatment for P3MT($TBACF_3SO_3$) NWs.

(8) Study of mismatch for P3MT($TBACF_3SO_3$) NWs.

Experimental Procedure

Sample preparation**:** The light-emitting P3MT NWs were synthesized using an electrochemical polymerization method based on an anodic alumina oxide (Al_2O_3) nanoporous template. The Al_2O_3 nanoporous templates (pore diameter of ~200 nm and thickness of 60 μm) were purchased from Whatman Co. The electrolyte used to synthesize of the P3MT NWs consisted of 3-methylthiophene (3MT) as a monomer, dodecylbenzne

sulfonic acid (DBSA) or tetrabutylammonium trifluoromethan sulfonic acid ($TBACF_3SO_3$) as a dopant, and acetonitrile (CH_3CN) as a solvent. The monomer to dopant molar ratio was 5:1. Without an additional dedoping process, the electrochemically synthesized P3MT NWs were in the lightly doped-states because of the dopant-assisted polymerization method, which was confirmed by the UV/Vis absorption spectra.[1,2] After synthesis of the P3MT NWs, a 2M HF or 2M NaOH solution was used to dissolve the Al_2O_3 nanoporous template. The NaOH solvent treatment of the electrochemically polymerized P3MT NWs induced dedoping states through a counter-ions exchanging process.[1, 2]

DNA hybridizations: The anthrax lethal factor DNA sequence was used as the *p*-DNA (NH_2-5`-ATC CTT ATC AAT ATT TAA CAA TAA TCC-3`) at concentrations of 100 nM. To couple the *p*-DNA with the P3MT NW, an amine group was attached to the 5`-end of the *p*-DNA sequence. The *p*-DNA was diluted with DI water (with the initial resistivity of 18 MΩ·cm Milli-Q water purifier), and the immobilization of *p*-DNA onto P3MT NWs was performed for 10 min with constant stirring. The sequences for the complementary *t*-DNA and 1-mer mismatched *t*-DNA were 3`-TAG GAA TAG TTA TAA ATT GTT ATT AGG-5`and 3`-TAG GAA TAG TTA TAA A**A**T GTT ATT AGG-5`, respectively. The hybridization reaction of *t*-DNA was accomplished for 10 min in a PBS stock buffer at pH=7.4. DI water was used to prepare the buffer solutions from the PBS stock buffer. All samples were dried in a vacuum oven for 30 min to allow measurement solid-state optical spectra under dry conditions.

Measurements: The formation of the P3MT NWs was visualized by SEM (JEOL JSM-5200). The optical characteristics of the P3MT NWs and DNA-functionalized P3MT NWs, which were dispersed homogeneously in a chloroform ($CHCl_3$) solution, were examined by

UV/Vis (HP-8453) absorption spectroscopy. FT-IR spectroscopy (Perkin-Elmer GX1) was used to analyze the structural properties of the nanosystems. The luminescence color CCD images of the NWs were measured using an AVT Marlin F-033C (λ_{ex} = 435 nm). The exposure time of the light was fixed at 1 sec to compare the brightness of the CCD images under the same experimental conditions. The solid (i.e., under dry conditions) PL images and spectra for an isolated single NW strand was measured using a LCM built around an inverted optical microscope (Axiovert 200, Zeiss GmbH). The 488 nm line of an unpolarized argon ion laser was used for LCM PL excitation. The spot size of the focused laser beam on the sample was estimated to be approximately 190 nm. The laser power incident on the sample and the acquisition time for each PL spectrum were fixed in the LCM PL measurements at 1 μW and 1 sec, respectively. Detailed methods for the LCM PL experiments were reported previously.[3-5]

Figure S1a shows the schematic chemical structures of P3MT, DBSA, and $TBACF_3SO_3$ materials. Figures S1b and c show the side and top-view SEM images, respectively, of the P3MT(DBSA) NWs after removing the Al_2O_3 template using an aqueous hydrofluoric acid (HF) solution. The length and diameter of the P3MT(DBSA) NWs were approximately 40 μm and 200 nm, respectively. Figures S1d and e show the side and top-view SEM images, respectively, of the P3MT($TBACF_3SO_3$) NWs after removing the Al_2O_3 template using a HF aqueous solution. The length and diameter of the P3MT($TBACF_3SO_3$) NWs were approximately 35 μm and 200 nm, respectively.

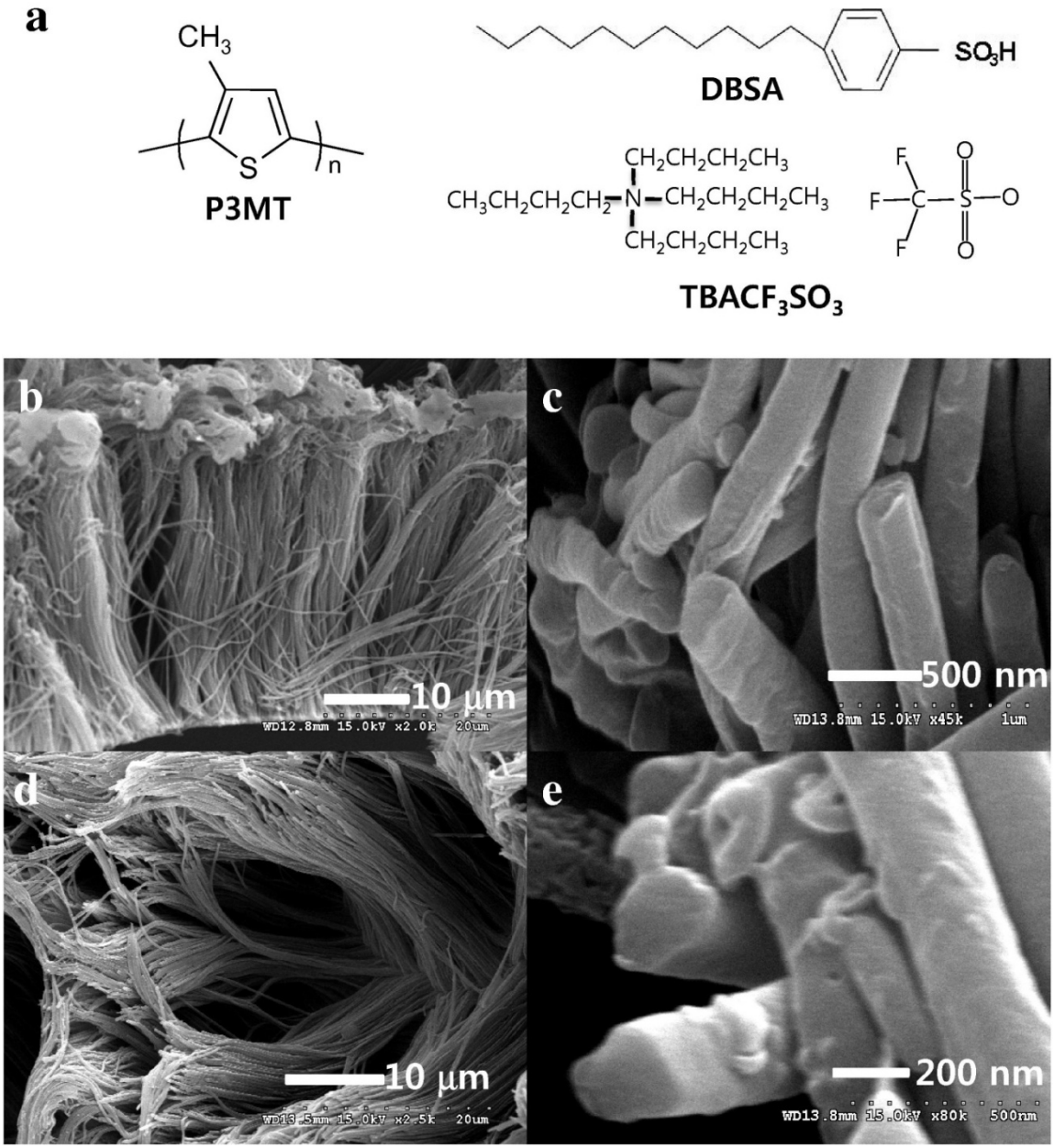

Figure S1. (a) Schematic chemical structures of the monomer unit of P3MT, DBSA, and $TBACF_3SO_3$ materials. (b, c) Side and top-view SEM images of the P3MT(DBSA) NWs, respectively. (d, e) Side and top-view SEM images of the P3MT($TBACF_3SO_3$) NWs, respectively.

Figure S2 shows the FT-IR spectra of *p*-DNA, *t*-DNA, and *p*-DNA+*t*-DNA in the range, 750 ~ 1310 cm^{-1}. The structural properties of carbohydrate and phosphodiester consisting of a backbone of DNA can be characterized by FT-IR spectroscopy.[6] For *p*-DNA, *t*-DNA and *p*-DNA+*t*-DNA, the phosphate backbone peaks at 1063, 1069, and 1070 cm^{-1} were assigned to the symmetric PO_2^- stretching vibration modes, and those at 1218, 1221, and 1225 cm^{-1} were assigned to the asymmetric PO_2^- stretching vibration modes. The symmetric C-O-P stretching vibration peaks of *p*-DNA, *t*-DNA and *p*-DNA+*t*-DNA was observed at 1149 cm^{-1}. Table S1 lists the assignments of the FT-IR characteristic peaks of the *p*-DNA, *t*-DNA and *p*-DNA+*t*-DNA.

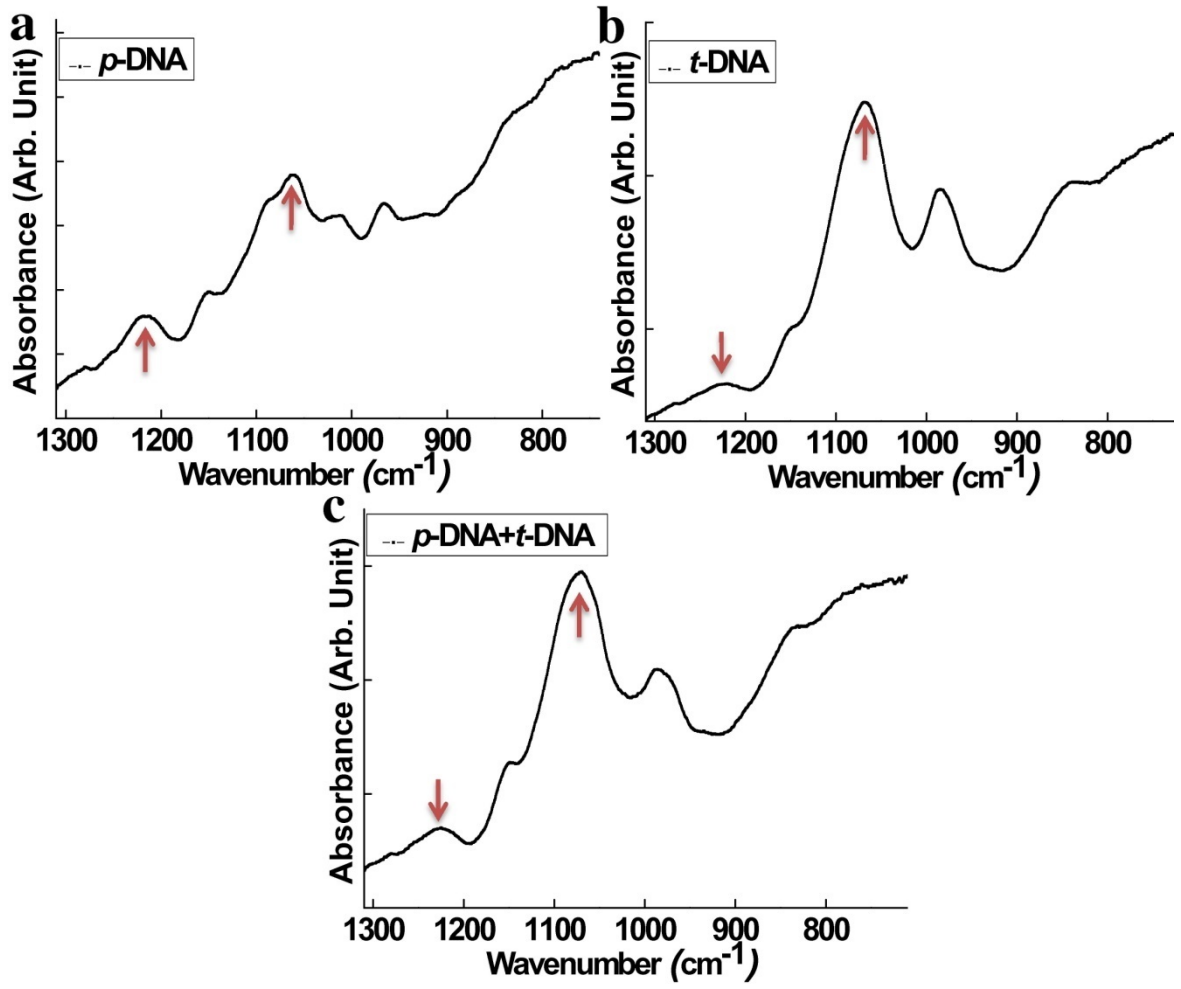

Figure S2. FT-IR spectra of (a) *p*-DNA, (b) *t*-DNA, and (c) *p*-DNA+*t*-DNA.

Table S1. Assignments of the FT-IR characteristic peaks of the *p*-DNA, *t*-DNA, and *p*-DNA+*t*-DNA.

Peak assignments	Wavenumber (cm^{-1})		
	p-DNA	*t*-DNA	*p*-DNA+*t*-DNA
asymmetric PO_2^- stretching vibration modes	1218	1221	1225
symmetric C-O-P stretching vibration modes	1149	1149	1149
symmetric PO_2^- stretching vibration modes	1063	1069	1070
not assigned	970	985	988
asymmetric O-P-O stretching vibration modes	830	838	830

Figure S3 shows the FT-IR spectra of the P3MT(DBSA), P3MT(DBSA)/*p*-DNA, and P3MT(DBSA)/*p*-DNA+*t*-DNA NWs. The IR characteristic vibration peaks for P3MT structures were observed. The vibration peaks due to out-of-plane C-H deformation were observed at 620 and 835 cm^{-1}, which were associated with the β position of the 3-methylthiophene (3-MT) ring. The peak at 736 cm^{-1} corresponds to the out-of-plane C-H bending vibration at the α position of the 3-MT ring (Fig. S3a). Relatively strong doping-induced vibration peaks were observed as *T* modes (translation modes) at 965, 1166, 1207, and 1299 cm^{-1} due to the DBSA dopant (Fig. S3b).[7,8] An additional doping-induced peaks were also found as *R* modes (ring deformation modes) at 544, 580, 710, and 860 cm^{-1} (Fig. S3a).

The doping-induced vibration peaks as *T* modes of the P3MT(DBSA)/*p*-DNA and P3MT(DBSA)/*p*-DNA+*t*-DNA NWs were still observed at approximately 972, 1172, 1207, and 1305 cm^{-1} and at approximately 978, 1175, 1209, and 1305 cm^{-1}, respectively (Fig. S3b). In addition, the doping-induced vibration peaks as *R* modes of the P3MT(DBSA)/*p*-DNA and P3MT(DBSA)/*p*-DNA+*t*-DNA NWs were observed at approximately 545, 582, 710 and 860 cm^{-1}, and at approximately 546, 582, 713 and 860 cm^{-1}, respectively (Fig. S3a). For the P3MT(DBSA)/*p*-DNA and P3MT(DBSA)/*p*-DNA+*t*-DNA NWs, additional peaks were observed at 1082 and 1246 cm^{-1} due to the DNA, which were assigned to the symmetric and asymmetric PO_2^- stretching vibration modes, respectively. The IR peaks positions were shifted to a high wavenumber when the P3MT(DBSA) NWs were functionalized with *p*-DNA and *t*-DNA. This shift is indicative of a change or rearrangement in the DNA backbone, which could be associated with an alternation of the phosphate group along the backbone of the DNA due to DNA hybridization with the P3MT(DBSA) NWs.

The FT-IR characteristics peaks in the ranges of 2800~3100 cm^{-1} are related to the methyl deformation modes. The intensities of the IR peaks of the P3MT(DBSA) NWs were relatively weak, whereas those of the P3MT(DBSA)/*p*-DNA and P3MT(DBSA)/*p*-DNA+*t*-DNA NWs were clearly enhanced (Fig. S3c). These results support the conformational modification of the P3MT main chain from a coil-like dominant configuration to a rod-like dominant configuration through DNA hybridization with the P3MT(DBSA) NW.[9,10] Table S2 lists the detailed assignments of the FT-IR characteristic peaks. The successful DNA functionalization of the P3MT NWs was confirmed based upon the peak assignments for the FT-IR spectra.

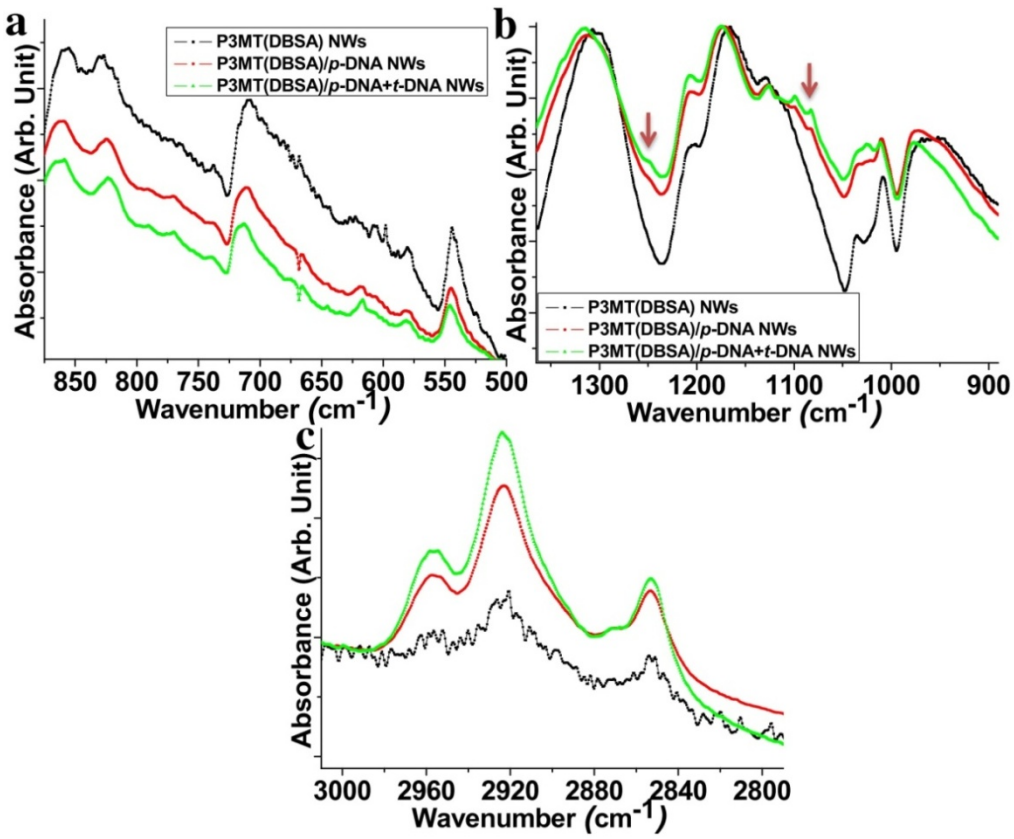

Figure S3. FT-IR spectra of the P3MT(DBSA), P3MT(DBSA)/*p*-DNA, and P3MT(DBSA)/*p*-DNA+*t*-DNA NWs in the ranges of (a) 500 ~ 880 cm^{-1}, (b) 880 ~ 1370 cm^{-1}, and (c) 2750 ~ 3010 cm^{-1}.

Table S2. Assignments of the FT-IR characteristic peaks of the P3MT(DBSA), P3MT(DBSA)/*p*-DNA, and P3MT(DBSA)/*p*-DNA+*t*-DNA NWs.

Peak assignments	Wavenumber (cm^{-1})		
	P3MT(DBSA) NWs	P3MT(DBSA)/ *p*-DNA NWs	P3MT(DBSA)/ *p*-DNA+*t*-DNA NWs
C_α-H out of-plane bending	735	736	736
C_β-H out of-plane bending	826	825	823
C_β-H in-plane bending	1009	1010	1012
C-C stretching	1207	1207	1209
C=C stretching	1299	1313	1314
Methyl **C-H** in-plane bending	1387	1394	1394
Ring stretching	1455	1459	1458
Doping-induced peaks (*T* modes)	965, 1166, 1207, 1299	972, 1172, 1207, 1305	978, 1175, 1209, 1305
Doping-induced peaks (*R* modes)	544, 580, 710, 860	545, 582, 710, 860	546, 582, 713, 860
methyl deformation modes	2851, 2921, 2958	2851, 2920, 2958	2852, 2921, 2958
asymmetric PO_2^- stretching vibration modes	×	1246	1246
symmetric PO_2^- stretching vibration modes	×	1082	1082

× : not observed

Figure S4 shows the three-dimensional (3-D) LCM PL images of the P3MT(DBSA), P3MT(DBSA)/*p*-DNA, and P3MT(DBSA)/*p*-DNA+*t*-DNA NW single NWs, which were measured under the same LCM experimental conditions. The average voltages of the LCM PL intensities for the as-prepared P3MT(DBSA), P3MT(DBSA)/*p*-DNA, and P3MT(DBSA)/*p*-DNA+*t*-DNA single NWs were 11±2 mV, 10±1 mV, and 61±3 mV, respectively. The LCM PL intensity of the functionalized P3MT(DBSA)/*p*-DNA+*t*-DNA single NW was approximately six times higher than that of the as-prepared P3MT(DBSA) single NW. The PL enhancement based on the 3-D LCM PL images of the P3MT(DBSA)/*p*-DNA+*t*-DNA NW is in good agreement with the CCD images (Fig. 1).

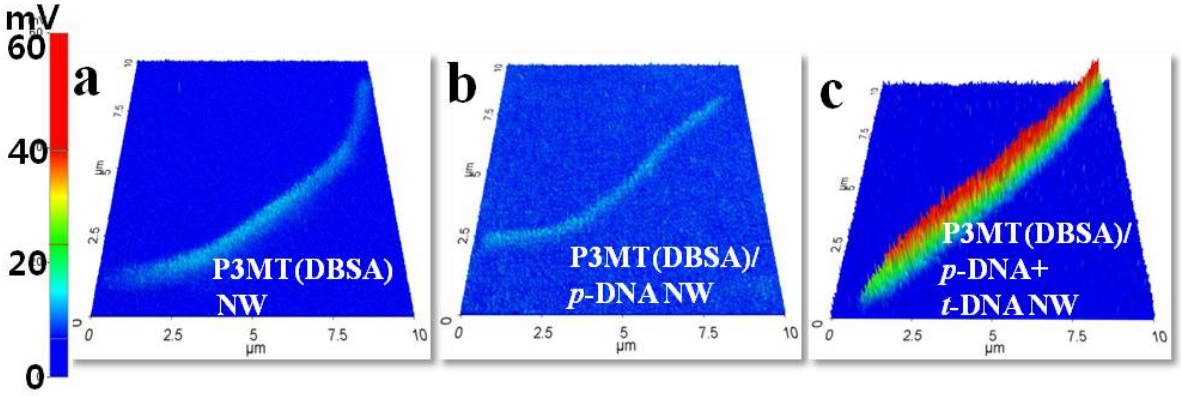

Figure S4. 3-D LCM PL images of a single strand of a) P3MT(DBSA), b) P3MT(DBSA)/*p*-DNA, and c) P3MT(DBSA)/*p*-DNA+*t*-DNA NWs.

The quantum yields (Φ_{QY}'s) of the P3MT(DBSA), P3MT(DBSA)/*p*-DNA, and P3MT (DBSA)/*p*-DNA+*t*-DNA NWs were measured to confirm the enhancement of PL intensity through *t*-DNA hybridization. To measure the Φ_{QY} of the NWs dispersed in $CHCl_3$ solution, the excitation wavelength was 400 nm. Coumarin 307 dissolved in methyl alcohol (Φ_{QY} =0.89) was used as a reference. The equation, $\Phi_{QY} = \Phi_{ST}\left(\frac{Grad_x}{Grad_{ST}}\right)\left(\frac{\eta_x^2}{\eta_{ST}^2}\right)$, was used. Subscripts *ST* and *X* denote the standard sample (Coumarin 307) and measured NWs, respectively. *Grad* means the gradient of the plot of the integrated area of the fluorescence intensity versus the absorbance of the π-π* transition peak. η is the refractive index of the solution. Figure S5 presents the plots of the integrated fluorescence intensity as a function of UV/Vis absorbance to estimate Φ_{QY}. The gradients of the P3MT(DBSA), P3MT(DBSA)/*p*-DNA, P3MT(DBSA)/*p*-DNA+*t*-DNA (1-mer mismatch), and P3MT(DBSA)/*p*-DNA+*t*-DNA (perfect match) NWs were estimated to be ~4.71×10^4, ~3.50×10^4, ~6.33×10^4, and ~1.55×10^5, respectively. Therefore, the calculated Φ_{QY} of the P3MT(DBSA)/*p*-DNA+*t*-DNA, P3MT(DBSA), and P3MT(DBSA)/*p*-DNA NWs was ~0.121, ~0.038 and 0.029, respectively, indicating about three-fold increase in Φ_{QY} after the hybridizing *t*-DNA. When 1-mer mismatched *t*-DNA were used, the Φ_{QY} of P3MT(DBSA)/*p*-DNA+*t*-DNA (1-mer mismatched) NWs was measured to be ~ 0.051 due to the less effective FCR. These results support the enhanced PL efficiency of the P3MT NWs after hybridizing the *t*-DNAs.

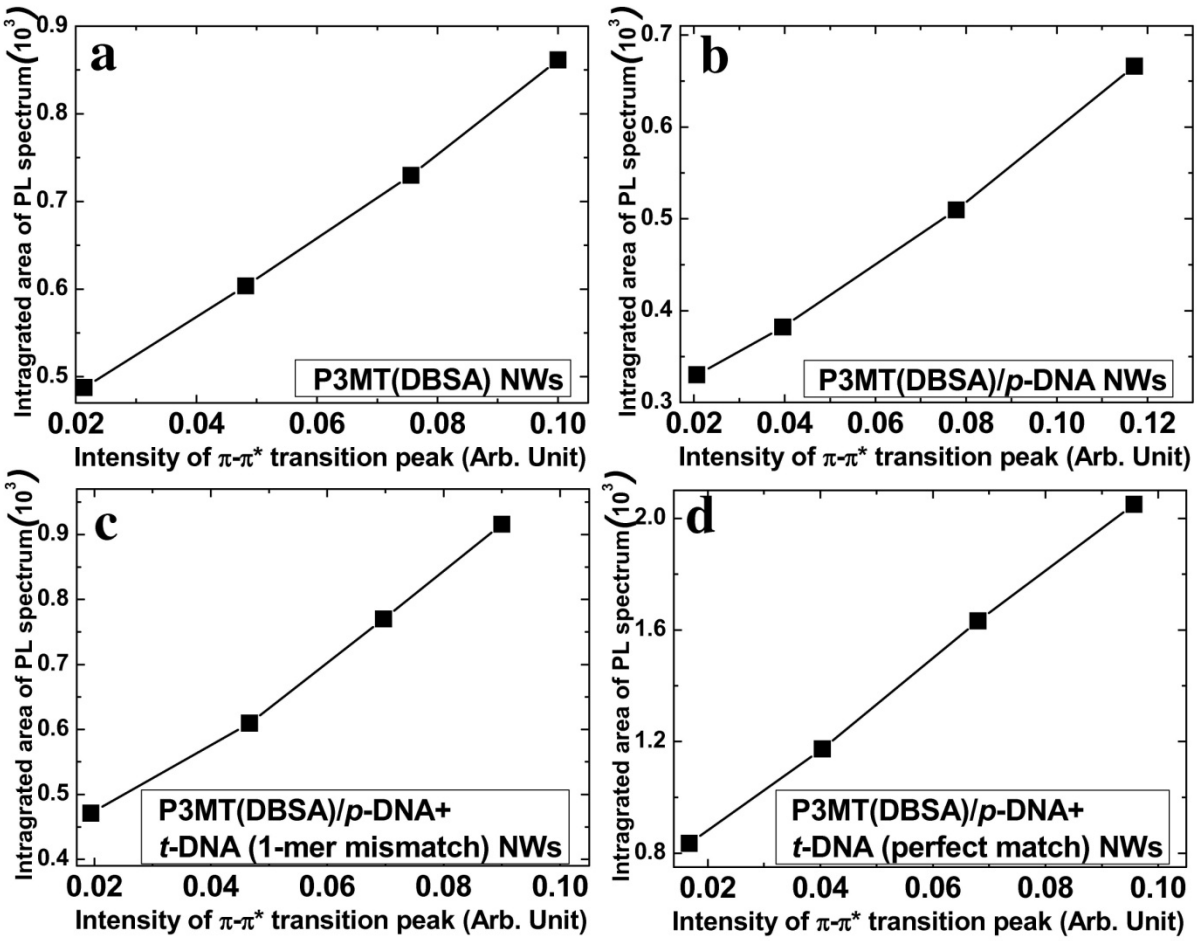

Figure S5. Plot of the integrated fluorescence intensity as a function of the UV/Vis absorbance intensity for (a) P3MT(DBSA) NWs, (b) P3MT(DBSA)/*p*-DNA NWs, (c) P3MT(DBSA)/*p*-DNA+*t*-DNA (1-mer mismatch) NWs, and (d) P3MT(DBSA)/*p*-DNA+*t*-DNA (perfect match) NWs.

An isolated single strand of dedoped-P3MT NW and their DNA-functionalized NWs were used to confirm the dopant-mediated FCR effect. The doping states of P3MT NWs can be controlled by the electrochemical methods or by a treatment with organic solvents, such as HF or NaOH during removal of the Al_2O_3 nanoporous template.[1,2] Relatively dedoped-P3MT NWs were obtained through counter-ion exchange using a NaOH treatment. From the normalized UV/Vis absorption spectra (Fig. S6a), the π-π* transition peak of the as-prepared dedoped-P3MT NW was observed at 415 nm and the broad bipolaron peak was not observed, suggesting the P3MT material has dedoped states.[11] The UV/Vis absorption bands, including the π-π* transition peak of the dedoped-P3MT, dedoped-P3MT/*p*-DNA, and dedoped-P3MT/*p*-DNA+*t*-DNA NWs, were similar (Fig. S6a). Figure S6b shows the LCM PL spectra of an isolated single strand of dedoped-P3MT, dedoped-P3MT/*p*-DNA, and dedoped-P3MT/*p*-DNA+*t*-DNA NWs obtained under the same LCM experimental conditions. Two main LCM PL peaks for a single strand of dedoped-P3MT NWs were detected at about 644 and 675 nm (i.e., red emission). The main LCM PL peaks of a single strand of dedoped-P3MT/*p*-DNA and dedoped-P3MT/*p*-DNA+*t*-DNA NWs were still observed at about 642 and 675 nm (i.e., red emission). The maximum LCM PL peak intensity and its integrated area of the single strand of *t*-DNA-hybridized dedoped-P3MT NW increased slightly (1.6 times) compared to those of the as-prepared dedoped-P3MT NWs, indicating a weak FCR effect.

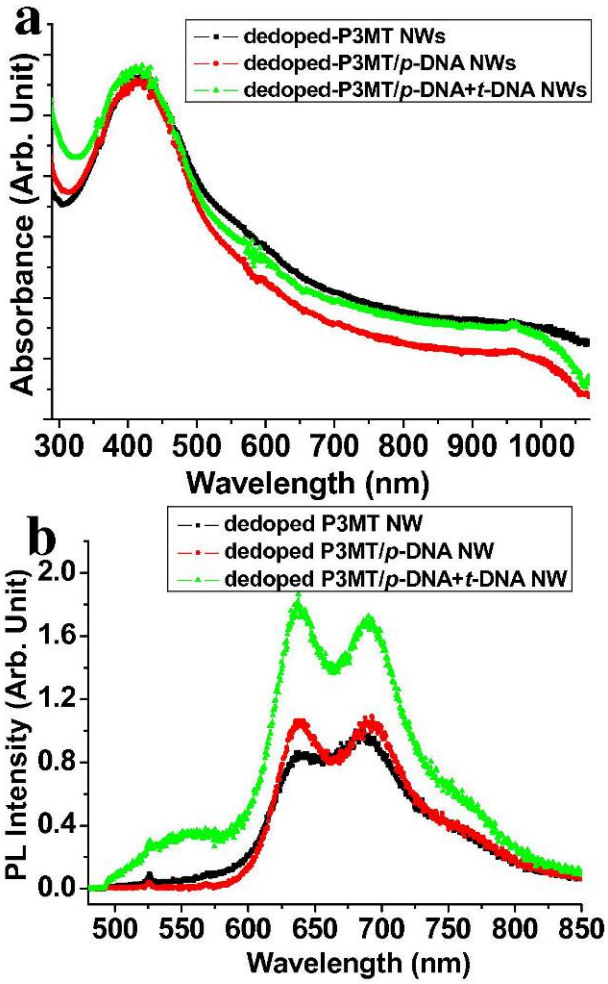

Figure S6. (a) Normalized UV/Vis absorption spectra of the dedoped-P3MT, dedoped-P3MT/*p*-DNA, and dedoped-P3MT/*p*-DNA+*t*-DNA NWs. (b) LCM PL spectra of a single strand of the NWs.

To investigate solvent effects, we measured the LCM PL spectra and color CCD images of P3MT NWs treated with solvents only, such as deionized (DI) water and phosphate-buffered saline (PBS) solution without DNA, under the same experimental conditions. Figures S7a-f show color CCD images of a bundle of the NWs for pristine P3MT($TBACF_3SO_3$), DI water treated P3MT($TBACF_3SO_3$), PBS treated P3MT($TBACF_3SO_3$), P3MT($TBACF_3SO_3$)/*p*-DNA, PBS treated P3MT($TBACF_3SO_3$)/*p*-DNA, and P3MT($TBACF_3SO_3$)/*p*-DNA+*t*-DNA, respectively. We observed a weak green light emission from a bundle of pristine P3MT($TBACF_3SO_3$) NWs. With the treatment of DI water and PBS solution without DNA, the luminescence color of a bundle of P3MT($TBACF_3SO_3$) NWs was still a weak green (Fig. S7b and c). When P3MT($TBACF_3SO_3$) NWs were coupled with *p*-DNA, the luminescence color changed from a green to a red with slightly decreased luminescence intensity (Fig. S7d). When P3MT($TBACF_3SO_3$)/*p*-DNA NWs were treated with PBS buffer solution without *t*-DNA, the luminescence color was still red and its intensity was almost the same as that before PBS treatment (Fig. S7e). The luminescence color of a bundle of P3MT($TBACF_3SO_3$)/*p*-DNA+*t*-DNA NWs showed significantly brighter red light emission compared to the P3MT($TBACF_3SO_3$)/*p*-DNA NWs, due to the FCR effect (Fig. S7f and Supplementary Movie).

Figure S7g compares the LCM PL spectra of the NWs of P3MT($TBACF_3SO_3$), DI water treated P3MT($TBACF_3SO_3$), PBS treated P3MT($TBACF_3SO_3$), P3MT($TBACF_3SO_3$)/*p*-DNA, PBS treated P3MT($TBACF_3SO_3$)/*p*-DNA, and P3MT($TBACF_3SO_3$)/*p*-DNA+*t*-DNA. The LCM PL spectra were measured for 100 different positions in the corresponding NWs and then presented average ones. For quantitative analysis, the maximum intensity of the LCM PL spectrum of the P3MT($TBACF_3SO_3$) NW was used as the reference unit. The LCM PL

peaks for a bundle of P3MT($TBACF_3SO_3$) NWs were detected at ~550 nm (Fig. S7g). The sharp peaks at 525 and 570 nm were due to Raman modes. The LCM PL peak positions of P3MT($TBACF_3SO_3$) NWs after the treatment of DI water or PBS solution were unchanged, as shown in Figure S7g. These suggest that the PL characteristics of P3MT($TBACF_3SO_3$) NWs were not changed by the DI water and PBS solution during the reaction time of 10 min. The LCM PL peaks for a bundle of P3MT($TBACF_3SO_3$)/*p*-DNA NWs were observed at about 645 and 680 nm (Fig. S7g). For the PBS treated P3MT/*p*-DNA NWs, the positions of LCM PL peaks were the same. After hybridized of a bundle of P3MT($TBACF_3SO_3$)/*p*-DNA NWs with *t*-DNAs, the luminescence intensity of the NWs was significantly enhanced as compared with other NWs, as shown in the inset of the Figure S7g. The results of PL characteristics for a bundle of P3MT($TBACF_3SO_3$) NWs hybridized with *p*-DNAs and *t*-DNAs were qualitatively similar to those of the P3MT($TBACF_3SO_3$) single NW. We also observed the similar LCM PL results for P3MT NWs doped with DBSA. The results indicate that the variations of luminescence color and intensity of the P3MT NWs are due to the hybridization with *p*-DNAs and *t*-DNAs, not due to the solvents such as DI water and PBS solution.

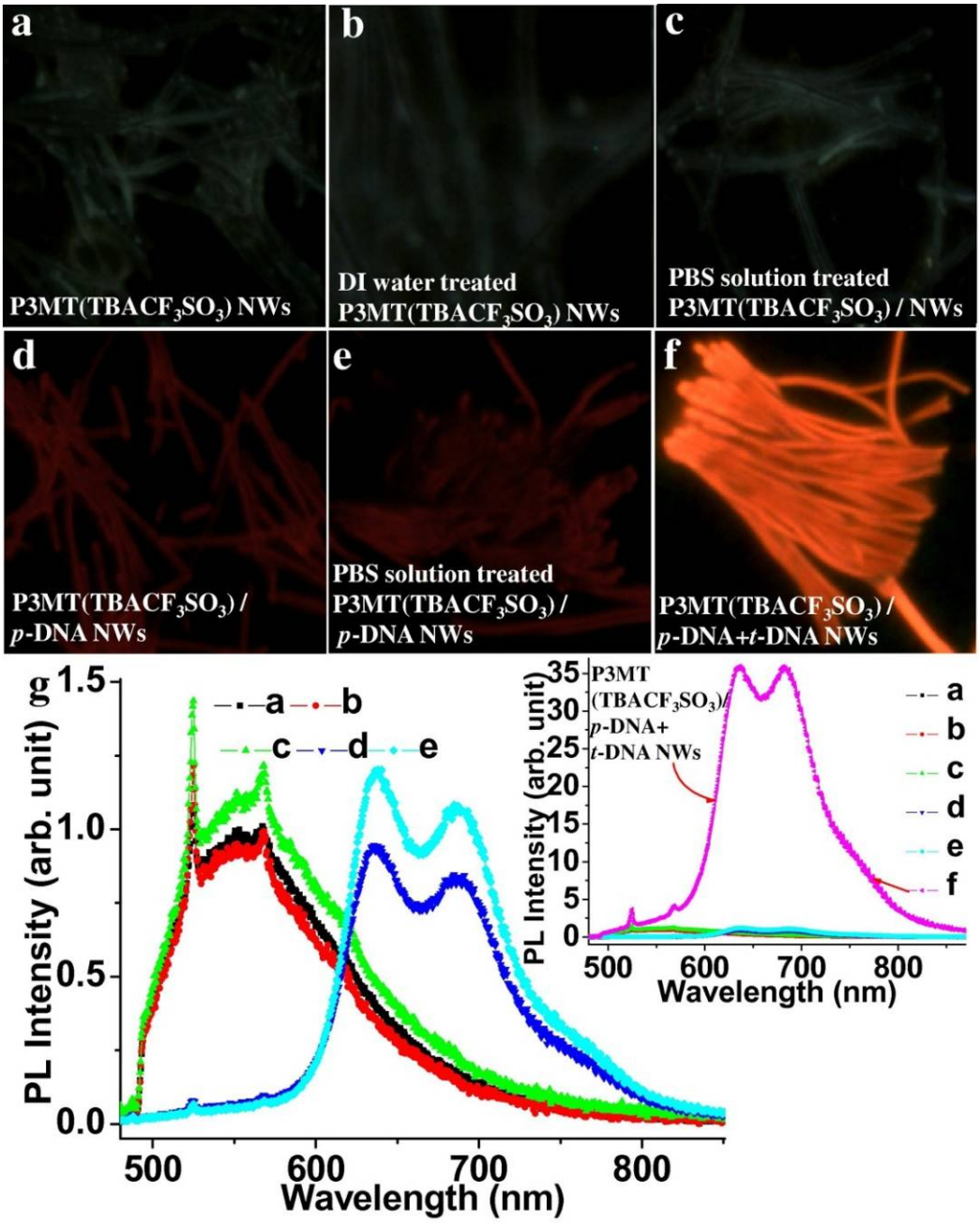

Figure S7. Color CCD images of a bundle of the NWs for (a) P3MT($TBACF_3SO_3$), (b) DI water treated P3MT($TBACF_3SO_3$), (c) PBS solution treated P3MT($TBACF_3SO_3$), (d) P3MT($TBACF_3SO_3$)/*p*-DNA, (e) PBS solution treated P3MT($TBACF_3SO_3$)/*p*-DNA, and (f) P3MT($TBACF_3SO_3$)/*p*-DNA+*t*-DNA. (g) LCM PL spectra of the NWs of **a.** P3MT($TBACF_3SO_3$), **b.** DI water treated P3MT($TBACF_3SO_3$), **c**. PBS treated P3MT($TBACF_3SO_3$), **d**. P3MT($TBACF_3SO_3$)/*p*-DNA, and **e**. PBS treated P3MT($TBACF_3SO_3$)/*p*-DNA. Inset: Comparison of LCM PL spectra of P3MT($TBACF_3SO_3$)/*p*-DNA+*t*-DNA NWs with other NWs presented in Fig. S7g.

We studied the variation in luminescence characteristics of P3MT($TBACF_3SO_3$) NWs using 1-mer mismatched *t*-DNAs with the different concentration of 1 pM. When the *p*-DNAs were coupled with 1-mer mismatched *t*-DNA (1 pM), the luminescence intensity of the LCM PL spectra of P3MT($TBACF_3SO_3$)/*p*-DNA+*t*-DNA (1-mer mismatch; 1pM) NW was much weaker than that of the perfect match case. The LCM PL intensities of the NWs hybridized with perfect match and 1-mer mismatch *t*-DNAs (with the concentration of 1 pM) were about 20 and 2 times, respectively, higher than those of the *p*-DNA functionalized NWs (Fig. S8). From these results, we confirmed the increase in PL efficiency of the P3MT/*p*-DNA+*t*-DNA NWs through the dopant-mediated FCR effect. In the case of 1-mer mismatch, the FCR effect became less effective between the light-emitting P3MT NWs and the *t*-DNA.

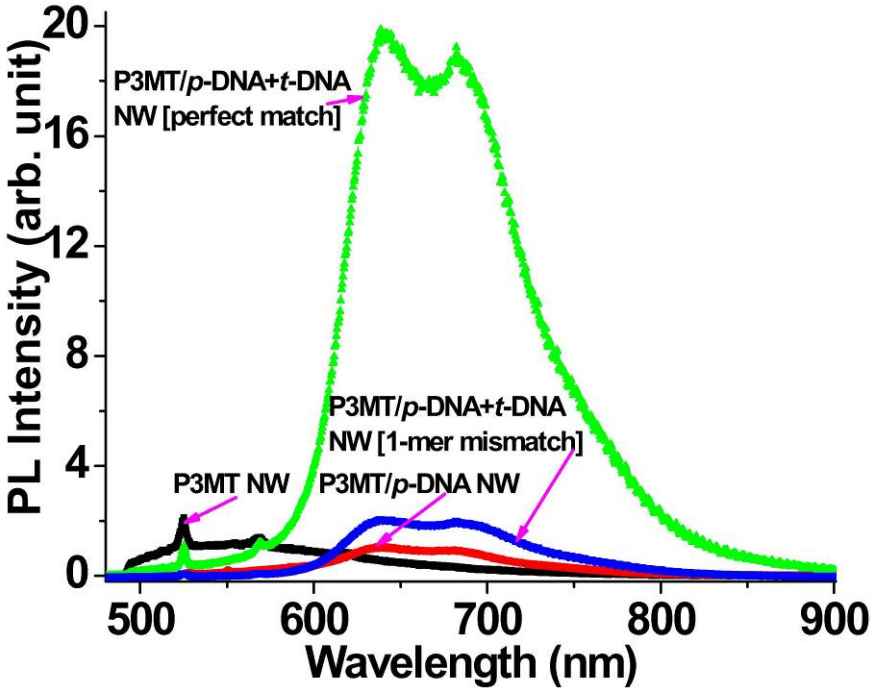

Figure S8. Comparison of LCM PL spectra of a P3MT($TBACF_3SO_3$), P3MT($TBACF_3SO_3$) /*p*-DNA, P3MT($TBACF_3SO_3$)/*p*-DNA+*t*-DNA (1-mer mismatch; 1 pM concentration) and P3MT($TBACF_3SO_3$) /*p*-DNA+*t*-DNA (perfect match; 1 pM concentration) single NW.

References

(1) D. H. Park, B. H. Kim, M. G. Jang, K. Y. Bae and J. Joo, *Appl. Phys. Lett*., 2005, **86**, 113116.

(2) D. H. Park, B. H. Kim, M. G. Jang, K. Y. Bae, S. J. Lee and J. Joo, *Synth. Met*., 2005, **153**, 341.

(3) D. H. Park, M. S. Kim and J. Joo, *Chem. Soc. Rev.,* 2010, **39**, 2439.

(4) Y. K. Hong, D. H. Park, S. K. Park, H. Song, D. -C. Kim, J. Kim, Y. H. Han, O. K. Park, B. C. Lee and J. Joo, *Adv. Funct. Mater*., 2009, **19**, 567.

(5) H. J. Kim, D. C. Kim, R. Kim, J. Kim, D. H. Park, H. S. Kim, J. Joo and Y. D. Suh, *J. Appl. Phys*., 2007, **101**, 053514.

(6) C. D. Kanakis, P. A. Tarantilis, C. Pappas, J. Bariyanga, H. A. Tajmir-Riahi and M. G. Polissiou, *J. Photochem. Photobio. B*, 2009, **95**, 204.

(7) Z. W. Sun and A. J. Frank, *J. Chem. Phys*., 1991, **94**, 4600.

(8) G. Tourillon and F. J. Garnier, *J. Phys. Chem*., 1983, **87**, 2289.

(9) Y. K. Hong, D. H. Park, S. H. Park, S. K. Park and J. Joo, *Appl. Phys*. *Lett*., 2009, **94**, 05311.

(10) O. Inganäs, K. Peter and R. Nilsson, *Nat. Mater*., 2003, **2**, 419.

(11) D. H. Park, H. S. Kim, M. -Y. Jeong, Y. B. Lee, H. -J. Kim, D. -C. Kim, J. Kim and J. Joo, *Adv. Funct. Mater.,* 2008, **18**, 2526.